PERGAMON

Journal of the Mechanics and Physics of Solids
47 (1999) 297–324

JOURNAL OF THE
MECHANICS AND
PHYSICS OF SOLIDS

Strain gradient crystal plasticity: size-dependent deformation of bicrystals

John Y. Shu[a,*], Norman A. Fleck[b]

[a] *Engineering Department, Lawrence Livermore National Laboratory, Livermore, CA 94550, U.S.A.*
[b] *Engineering Department, University of Cambridge, Trumpington Street, Cambridge CB2 1PZ, U.K.*

Received 26 January 1998; in revised form 19 June 1998

Abstract

The role of the grain boundary in influencing the deformation of a bicrystal is explored using a rate-dependent crystal formulation of the Fleck–Hutchinson strain gradient plasticity theory. The physical basis of the theory is the elevated strengthening of a slip system due to geometrically necessary dislocations, associated with spatial gradients of slip. The theory is implemented within the finite element framework and is used to study the deformation of a bicrystal under in-plane shear loading. Contrary to classical scale-independent crystal plasticity theories, the strain gradient theory predicts that the deformation state depends strongly upon grain size. Strain gradient effects are pronounced within a narrow layer at the grain boundary of a bicrystal, and a significant grain-size dependence of the yield strength is predicted.

Keywords: Grain boundaries; Strengthening mechanisms; Constitutive behaviour; Crystal plasticity; Non-local plasticity

1. Introduction

Conventional continuum mechanics theories assume that the stress at a material point depends upon variables such as strain at the same point only. This local assumption has long been shown to be adequate when the wavelength of the deformation field is much larger than the dominant length scale of the microstructure. Material behaviour predicted by such a local theory exhibits scale-independence: no length scale is present within the constitutive law. However, accumulating experimental evidence suggests that a strong size-dependence of mechanical behaviour

* Corresponding author. Tel.: 001 925 422 6333; fax: 001 925 423 0455; e-mail: jyshu@llnl.gov

S0022–5096/99/$ - see front matter
PII: S0022–5096(98)00081–7

exists at a length scale on the order of microns, see Fleck and Hutchinson (1997) for a topical review. Since early this century when Cosserat and Cosserat (1909) proposed a coupled stress theory, various non-local or strain gradient continuum theories have been proposed to include constitutive length scales in order to model material deformation more accurately at small scales or in regions of large strain gradient, see, for example, Aifantis (1984), Acharya and Bassani (1995), Fleck et al. (1994) and Fleck and Hutchinson (1993, 1997).

There has been a significant amount of work done in developing strain gradient theories, but most of them are phenomenological and for homogenised polycrystals. An exception is the study of Forest and Cailletaud (1995) who employed a couple stress theory to study strain localisation in single crystals. Although couple stress type theories have achieved some success in modelling size effects (see the reviews of William et al., 1995; Fleck and Hutchinson, 1997), they consider only the effect of gradient of rotation, and ignore the gradient of normal strain. Xia and Hutchinson (1996) used the couple-stress plasticity theory of Fleck and Hutchinson (1993) in an attempt to explain the occurrence of cleavage fracture at a mode I crack tip at a ceramic–metal interface. Conventional plasticity theory is unable to give sufficiently high levels of stress for cleavage fracture to be expected. Xia and Hutchinson found that the traction on the crack plane, directly ahead of a mode-I crack in the couple-stress solid, is only marginally higher than that given by the well-known HRR field for the conventional plastic solid. Shu and Fleck (1998) also used the Fleck–Hutchinson couple-stress plasticity theory to try to predict the size-dependent hardness of a metal polycrystal, for indents on the length scale of microns. The predicted increment in hardness with diminishing indent size falls short of the observed size effect. It was found in both studies that the deformation field is predominantly dilatational, rather than rotational in nature. Since couple-stress theory assumes that additional hardening arises only from rotation gradients, no significant size effect can thus be predicted.

Gradients of strain are included in the elastic–plastic strain gradient theory of Fleck and Hutchinson (1997). It makes use of all second-order gradients of displacements and fits within the general framework of Mindlin (1964). The phenomenological version of the Fleck and Hutchinson (1997) theory has been used successfully to predict enhanced stresses ahead of a crack tip compared with the conventional HRR solution (Wei and Hutchinson, 1997) and a significant size effect in cone indentation (Begley and Hutchinson, 1997). As an application of the crystal plasticity version of the theory, Smyshlyaev and Fleck (1996) explored the effect of grain size on the strength of a polycrystal. They considered a deformation theory version of plasticity with no partitioning between elastic and plastic strains. A compatible distribution of strain and strain gradient was obtained throughout the polycrystal. However, for a crystal obeying an elastic–plastic constitutive law, the existence of such solutions is not guaranteed, as will be explained further below. We get around this difficulty in the present paper by introducing additional kinematic freedom into the constitutive model.

In this paper, a rate-dependent strain gradient crystal plasticity theory is presented and used to examine shear deformation within a bicrystal, including the boundary

layer adjacent to the grain boundary. The theory is an extension of the Fleck and Hutchinson (1997) strain gradient plasticity theory and again leads to a grain size effect on strength. The paper is organised as follows.

In Section 2, we follow the general method laid down by Mindlin (1964) to develop a higher-order theory based on the notion of a representative microvolume. The microvolume provides the length scale in the constitutive law. The precise physical interpretation of this length scale remains unclear. Fleck et al. (1994) assume that the length scale is set by the free slip distance of dislocations; an alternative view is that the length scale is set by the dislocation cell size. Hopefully, this question will be answered soon by the explicit modelling of discrete dislocations, using methods developed by Kubin et al. (1992) and van der Giessen and Needleman (1995), for example. In this paper, 'micro' refers to the scale at which discrete dislocations are considered while 'macro' refers to a scale at which the material is viewed as a continuum with homogenised plastic deformation.

In Section 3, an elastic–viscoplastic formulation of the strain gradient crystal plasticity theory is presented. It is based on the idea that elevated hardening of slip resistance arises from geometrically necessary dislocations (Ashby, 1970). An application of the theory is reported in Section 4: we consider the plane-strain deformation of a lamellar bicrystal, and explore the effects of interface constraints on the deformation field. An attempt is made to reproduce the well-known Hall–Petch grain size effect.

Throughout this paper, a bold character denotes a vector or a tensor. Deformation is assumed to be infinitesimal, and rate-of-change with respect to time is denoted by an ascent dot. Repeated lower case Roman indices imply summation over the range 1–3.

2. Continuum description of crystal deformation at microscale and its homogenisation

The plastic deformation of metals is predominantly by the mechanism of dislocation glide. Due to the extremely large number of dislocations in a typical crystal, it is practically impossible using currently available computer power to keep track of each dislocation, and some sort of averaging procedure is needed to construct a macroscopic constitutive law.

Consider a macroscopically homogeneous continuum occupying a macro volume V. The macro Cartesian co-ordinate vector $\mathbf{X}$ is used to identify a macroscopic material point. A small but finite volume δV surrounding the macroscopic material point (see Fig. 1(a)) is referred to as a micro-volume. This micro-volume contains a 'microstructure' in the sense of a dislocation distribution. A material point within the micro-volume δV is identified by a micro Cartesian coordinate vector $\mathbf{x}$ with its origin at the centre of δV (see Fig. 1(b)).

We assume that the volume element δV comprises a crystal with a set of slip systems. Plastic straining of the micro-volume is by slip on these slips systems. The slip rate for each active system (α) is approximated by a first-order Taylor expansion

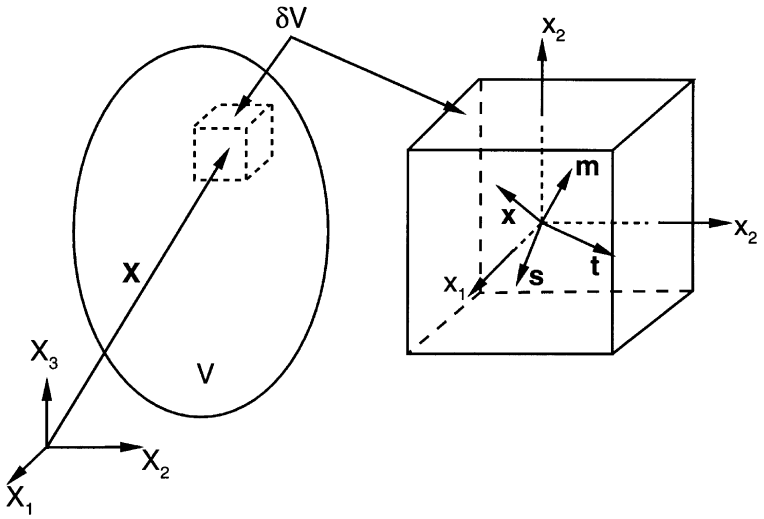

Fig. 1. (a) A sketch of a microscopic volume δV at a position $\mathbf{X}$ in a macroscopic continuum, (b) the local co-ordinate system $\mathbf{x}$ and slip system vectors in the micro volume δV.

$$\dot{\gamma}^{(\alpha)}(\mathbf{X},\mathbf{x}) \approx \bar{\dot{\gamma}}^{(\alpha)}(\mathbf{X}) + x_{\mathrm{S}}^{(\alpha)}\dot{\bar{\gamma}}_{\mathrm{S}}^{(\alpha)}(\mathbf{X}) + x_{\mathrm{T}}^{(\alpha)}\dot{\bar{\gamma}}_{\mathrm{T}}^{(\alpha)}(\mathbf{X}) + x_{\mathrm{M}}^{(\alpha)}\dot{\bar{\gamma}}_{\mathrm{M}}^{(\alpha)}(\mathbf{X}) \tag{2.1}$$

in terms of the local co-ordinate $\mathbf{x}$ via $x_{\mathrm{S}}^{(\alpha)} = s_k^{(\alpha)}x_k$, $x_{\mathrm{T}}^{(\alpha)} = t_k^{(\alpha)}x_k$ and $x_{\mathrm{M}}^{(\alpha)} = m_k^{(\alpha)}x_k$. In (2.1) and in the following,no summation is implied over the upper case labels (S, M, T). As shown in Fig. 1(b), the unit vectors $(\mathbf{s}^{(\alpha)}, \mathbf{t}^{(\alpha)}, \mathbf{m}^{(\alpha)})$ form a right-handed set of orthogonal directions and refer to the slip direction, the transverse direction and the direction normal to the slip plane, respectively. The parameter $\bar{\dot{\gamma}}^{(\alpha)}$ is the average slip rate over δV, $\dot{\bar{\gamma}}_{\mathrm{S}}^{(\alpha)}$ is the average local gradient of slip in the slip direction, and so on. The overall macroscopic plastic strain rate can be expressed as

$$\dot{\varepsilon}_{ij}^{\mathrm{p}}(\mathbf{X},\mathbf{x}) = \sum_{\alpha} \dot{\gamma}^{(\alpha)}(\mathbf{X},\mathbf{x})\mu_{ij}^{(\alpha)}(\mathbf{X}) \tag{2.2}$$

in which

$$\mu_{ij}^{(\alpha)} = (s_i^{(\alpha)}m_j^{(\alpha)} + s_j^{(\alpha)}m_i^{(\alpha)})/2 \tag{2.3}$$

is the classical Schmid orientation tensor. Here and elsewhere in this paper, summation is taken over all active slip systems (α) of the crystal. (For a rate-dependent crystal, summation is over all slip systems.) On the microscale, we further assume that the crystal is characterised by the classical framework of plasticity, i.e., plastic dissipation is by the Cauchy stress working through the plastic strain rate, and that higher-order stresses do not exist. The plastic energy dissipation rate per unit macro-volume is therefore

$$\dot{W}^{\mathrm{p}} \equiv \frac{1}{\delta V}\int_{\delta V} \sigma_{ij}\dot{\varepsilon}_{ij}^{\mathrm{p}}\,\mathrm{d}v \equiv \frac{1}{\delta V}\sum_{\alpha}\int_{\delta V} \tau^{(\alpha)}\dot{\gamma}^{(\alpha)}\,\mathrm{d}v \tag{2.4}$$

where $\tau^{(\alpha)} \equiv \sigma_{ij}\mu_{ij}^{(\alpha)}$ is the classical Schmid stress. Substituting (2.1) and (2.2) into the above equation and carrying out the volume integration of the dissipation rate, one obtains

$$\dot{W}^{\mathrm{p}} = \bar{\sigma}_{ij}\dot{\bar{\varepsilon}}_{ij}^{\mathrm{p}} + \bar{\tau}_{ijk}\dot{\bar{\eta}}_{ijk}^{\mathrm{p}} \tag{2.5}$$

in which

$$\dot{\bar{\varepsilon}}_{ij}^{\mathrm{p}} = \sum_{\alpha} \dot{\bar{\gamma}}^{(\alpha)}\mu_{ij}^{(\alpha)} \quad \text{and} \quad \dot{\bar{\eta}}_{ijk}^{\mathrm{p}} = \sum_{\alpha} (\dot{\bar{\gamma}}_{\mathrm{S}}^{(\alpha)} s_k^{(\alpha)} + \dot{\bar{\gamma}}_{\mathrm{T}}^{(\alpha)} t_k^{(\alpha)} + \dot{\bar{\gamma}}_{\mathrm{M}}^{(\alpha)} m_k^{(\alpha)})\mu_{ij}^{(\alpha)} \tag{2.6}$$

are the volume averages of plastic strain rate and the local gradient of plastic strain rate, respectively. The work conjugate quantities for $(\bar{\varepsilon}_{ij}^{\mathrm{p}}, \bar{\eta}_{ijk}^{\mathrm{p}})$ over the volume δV are defined by

$$\bar{\sigma}_{ij} \equiv \frac{1}{\delta V}\int_{\delta V} \sigma_{ij}\,\mathrm{d}v \quad \text{and} \quad \bar{\tau}_{ijk} \equiv \frac{1}{\delta V}\int_{\delta V} x_k\sigma_{ij}\,\mathrm{d}v \tag{2.7}$$

respectively. It is clear from the above relations that we can interpret $\bar{\sigma}_{ij}$ as the volume average of the microscopic Cauchy stress, and that $\bar{\tau}_{ijk}$ is the first moment of the Cauchy stress over δV. Following Mindlin (1964) and Fleck and Hutchinson (1997), we shall refer to $\bar{\tau}_{ijk}$ as a double stress.

Alternatively, the plastic dissipation rate per unit macro volume can be expressed in terms of local slips as

$$\dot{W}^{\mathrm{p}} = \sum_{\alpha} (\bar{\tau}^{(\alpha)}\dot{\bar{\gamma}}^{(\alpha)} + \bar{Q}_{\mathrm{S}}^{(\alpha)}\dot{\bar{\gamma}}_{\mathrm{S}}^{(\alpha)} + \bar{Q}_{\mathrm{T}}^{(\alpha)}\dot{\bar{\gamma}}_{\mathrm{T}}^{(\alpha)} + \bar{Q}_{\mathrm{M}}^{(\alpha)}\dot{\bar{\gamma}}_{\mathrm{M}}^{(\alpha)}) \tag{2.8}$$

in which

$$\bar{\tau}^{(\alpha)} \equiv \frac{1}{\delta V}\int_{\delta V} \tau^{(\alpha)}\,\mathrm{d}v \tag{2.9a}$$

is the average resolved shear stress and the quantities $(\bar{Q}_{\mathrm{S}}^{(\alpha)}, \bar{Q}_{\mathrm{T}}^{(\alpha)}, \bar{Q}_{\mathrm{M}}^{(\alpha)})$, defined by

$$\bar{Q}_{\mathrm{S}}^{(\alpha)} \equiv \frac{1}{\delta V}\int_{\delta V} x_{\mathrm{S}}^{(\alpha)}\tau^{(\alpha)}\,\mathrm{d}v, \quad \bar{Q}_{\mathrm{T}}^{(\alpha)} \equiv \frac{1}{\delta V}\int_{\delta V} x_{\mathrm{T}}^{(\alpha)}\tau^{(\alpha)}\,\mathrm{d}v, \quad \bar{Q}_{\mathrm{M}}^{(\alpha)} \equiv \frac{1}{\delta V}\int_{\delta V} x_{\mathrm{M}}^{(\alpha)}\tau^{(\alpha)}\,\mathrm{d}v \tag{2.9b}$$

are the resolved double stresses. It is transparent from (2.9b) that the resolved double stresses are the first-order moments of the microscopic Schmid stress.

The total strain rate $\dot{\varepsilon}_{ij}$ in the microvolume δV is the sum of the elastic and plastic parts, and is taken to be a linear distribution within δV. Thus, the total work rate in a unit macro volume can be written as

$$\dot{W} \equiv \frac{1}{\delta V}\int_{\delta V} \sigma_{ij}\dot{\varepsilon}_{ij}\,\mathrm{d}v = \bar{\sigma}_{ij}\dot{\bar{\varepsilon}}_{ij} + \bar{\tau}_{ijk}\dot{\bar{\eta}}_{ijk} \tag{2.10}$$

where

$$\bar{\dot{\varepsilon}}_{ij} = \frac{1}{\delta V}\int_{\delta V} \dot{\varepsilon}_{ij}\,\mathrm{d}v, \quad \bar{\dot{\eta}}_{ijk} = \frac{1}{\delta V}\int_{\delta V} \partial\dot{\varepsilon}_{ij}/\partial x_k\,\mathrm{d}v \tag{2.11}$$

are the average microscopic strain rate and average microscopic strain rate gradient, respectively. We make the choice that the average microscopic strain rate $\bar{\dot{\varepsilon}}_{ij}$ within δV equals the macroscopic strain rate at the same location $\mathbf{X}$; similarly, the average microscopic gradient of strain rate $\bar{\dot{\eta}}_{ijk}$ within δV equals the macroscopic gradient of strain rate at $\mathbf{X}$. Thus,

$$\bar{\dot{\eta}}_{ijk} \equiv \partial\bar{\dot{\varepsilon}}_{ij}/\partial X_k. \tag{2.12}$$

Note that the microscopic gradient of slip within δV need not to be the same as the macroscopic gradient of average slip: $\bar{\dot{\gamma}}_k^{(\alpha)} \neq \partial\bar{\dot{\gamma}}^{(\alpha)}/\partial X_k$ and $\bar{\dot{\eta}}_{ijk}^{\mathrm{p}} \neq \partial\bar{\dot{\varepsilon}}_{ij}^{\mathrm{p}}/\partial X_k$ in general.

In classical theories of plasticity, the higher-order double stress $\bar{\tau}_{ijk}$ is neglected. This practice is reasonable when the deformation and stress field wavelength is much larger than the size of the micro volume δV, but is questionable when the two scales are comparable, as discussed in the Introduction. Only the first-order gradient of strain is kept in the Fleck and Hutchinson (1997) plasticity framework and in the formulation presented below. In general, higher than first-order gradients of strain should also be included in order to model the effects of highly non-uniform microscopic detail; however, the inclusion of multiple gradients would make the constitutive law and numerical implementation impractical.

In order to formulate a complete theory of crystal plasticity with strain gradient effects, we shall write a virtual work statement in terms of macroscopic quantities. The internal work rate per unit volume in the $\mathbf{X}$ co-ordinate system is given by the right-hand side of (2.10). At each macroscopic point, the plastic work rate is given by (2.5) or equivalently by (2.8).

3. Elasto–viscoplastic strain gradient crystal plasticity

In this section, a rate formulation of a strain gradient crystal theory of plasticity is proposed. We shall work solely in terms of the macroscopic co-ordinate system $\mathbf{X}$ and the overbar quantities of the previous section; for simplicity of expression, we drop the use of the overbar notation hereafter.

3.1. Kinematics

The velocity gradient $\mathbf{L}$ is the spatial gradient of velocity $\mathbf{v}$ and is defined in component form as $L_{ij} = \partial v_i/\partial X_j$. Upon partitioning $\mathbf{L}$ into an elastic part and a plastic part, i.e., $\mathbf{L} = \mathbf{L}^{\mathrm{e}} + \mathbf{L}^{\mathrm{p}}$, the plastic part is related to the slip rates on each slip system by

$$L_{ij}^{\mathrm{p}} = \sum_{\alpha} \dot{\gamma}^{(\alpha)} s_i^{(\alpha)} m_j^{(\alpha)}. \tag{3.1}$$

Similarly, the plastic part of the total strain rate $\dot{\boldsymbol{\varepsilon}} \equiv (\mathbf{L}+\mathbf{L}^{\mathrm{T}})/2$ (a superscript T denotes transpose) is related to the slip rates via

$$\dot{\boldsymbol{\varepsilon}} = \sum_{\alpha} \dot{\gamma}^{(\alpha)} \boldsymbol{\mu}^{(\alpha)} \tag{3.2}$$

where the components of the tensor $\boldsymbol{\mu}^{(\alpha)}$ are given by (2.3). The third-order strain rate gradient tensor $\dot{\boldsymbol{\eta}}$ is defined in component form as $\dot{\eta}_{ijk} = \partial \dot{\varepsilon}_{ij}/\partial X_k$. The plastic part of the strain rate gradient can be expressed as

$$\dot{\boldsymbol{\eta}}^{\mathrm{p}} = \sum_{\alpha} \dot{\gamma}_{\mathrm{S}}^{(\alpha)} \boldsymbol{\psi}_{\mathrm{S}}^{(\alpha)} + \dot{\gamma}_{\mathrm{T}}^{(\alpha)} \boldsymbol{\psi}_{\mathrm{T}}^{(\alpha)} + \dot{\gamma}_{\mathrm{M}}^{(\alpha)} \boldsymbol{\psi}_{\mathrm{M}}^{(\alpha)} \tag{3.3}$$

in which the components of the tensors $\boldsymbol{\psi}_{\mathrm{S}}^{(\alpha)}$, $\boldsymbol{\psi}_{\mathrm{T}}^{(\alpha)}$ and $\boldsymbol{\psi}_{\mathrm{M}}^{(\alpha)}$ are given by

$$\psi_{\mathrm{S}ijk}^{(\alpha)} = s_k^{(\alpha)} \mu_{ij}^{(\alpha)}, \quad \psi_{\mathrm{T}ijk}^{(\alpha)} = t_k^{(\alpha)} \mu_{ij}^{(\alpha)} \quad \text{and} \quad \psi_{\mathrm{M}ijk}^{(\alpha)} = m_k^{(\alpha)} \mu_{ij}^{(\alpha)} \tag{3.4}$$

respectively. Here $\dot{\gamma}_{\mathrm{S}}^{(\alpha)}$, $\dot{\gamma}_{\mathrm{T}}^{(\alpha)}$ and $\dot{\gamma}_{\mathrm{M}}^{(\alpha)}$ are the microscopic slip gradients along the slip, transverse and slip plane normal directions, respectively, as explained in the previous section.

The plastic work rate per unit volume $\dot{W}^{\mathrm{p}}$ follows from (2.5) and (2.8) as

$$\dot{W}^{\mathrm{p}} = \sigma_{ij} \dot{\varepsilon}_{ij}^{\mathrm{p}} + \tau_{ijk} \dot{\eta}_{ijk}^{\mathrm{p}} = \sum_{\alpha} (\tau^{(\alpha)} \dot{\gamma}^{(\alpha)} + Q_{\mathrm{S}}^{(\alpha)} \dot{\gamma}_{\mathrm{S}}^{(\alpha)} + Q_{\mathrm{T}}^{(\alpha)} \dot{\gamma}_{\mathrm{T}}^{(\alpha)} + Q_{\mathrm{M}}^{(\alpha)} \dot{\gamma}_{\mathrm{M}}^{(\alpha)}) \tag{3.5}$$

where $\tau^{(\alpha)}$ is the classical Schmid stress while the resolved double stresses are

$$Q_{\mathrm{S}}^{(\alpha)} = \psi_{\mathrm{S}ijk}^{(\alpha)} \tau_{ijk}, \quad Q_{\mathrm{M}}^{(\alpha)} = \psi_{\mathrm{M}ijk}^{(\alpha)} \tau_{ijk} \quad \text{and} \quad Q_{\mathrm{T}}^{(\alpha)} = \psi_{\mathrm{T}ijk}^{(\alpha)} \tau_{ijk}. \tag{3.6}$$

Following Fleck and Hutchinson (1997), the principle of virtual work for the strain gradient material can be written as

$$\int_V [\sigma_{ij} \delta \dot{\varepsilon}_{ij} + \tau_{ijk} \delta \dot{\eta}_{ijk}] \, \mathrm{d}V = \int_{\mathrm{S}} [t_i \delta v_i + r_i D \delta v_i] \, \mathrm{d}S \tag{3.7}$$

for an arbitrary velocity increment $\delta \mathbf{v}$ upon neglecting body forces. Here, t_i and r_i are the traction and double stress traction per unit area of the surface S, respectively. The stress σ_{ij} and double stress τ_{ijk} satisfy the equilibrium relation

$$\sigma_{ij,j} - \tau_{ijk,jk} = 0 \tag{3.8}$$

within V, and on the surface S are in equilibrium with the tractions according to

$$t_i = n_j(\sigma_{ij} - \tau_{ijk,k}) + n_j n_k \tau_{ijk}(D_l n_l) - D_j(n_k \tau_{ijk}) \tag{3.9}$$

and

$$r_i = n_j n_k \tau_{ijk}. \tag{3.10}$$

In the above equations, a comma denotes a partial derivative. $D_j(\,) = (\delta_{jk} - n_j n_k)\, \partial(\,)/\partial X_k$ is a surface-gradient operator and $D(\,) = n_k(\,)/\partial X_k$ is the surface normal-gradient operator. The i-th component of the unit surface normal is n_i. Within the Fleck–Hutchinson framework of strain gradient plasticity theories, a

unique solution is obtainable only when six independent boundary conditions are prescribed, i.e. the three usual traction-velocity boundary conditions of either t_i or v_i and the three higher-order boundary conditions of either r_i or Dv_i.

3.2. Constitutive law

Before spelling out the constitutive equations for strain gradient crystal plasticity, we shall give a brief review of the constitutive law for a classical crystal plasticity theory (see for example, Peirce et al., 1983). In a classical rate-dependent formulation based on the Schmid law, the slip rate $\dot{\gamma}^{(\alpha)}$ on a slip system (α) is assumed to satisfy

$$\dot{\gamma}^{(\alpha)}/\dot{\gamma}_0 = F(\tau^{(\alpha)}/g^{(\alpha)}) \tag{3.11}$$

where $\dot{\gamma}_0$ is a reference slip rate, and F is a dimensionless function of the ratio of Schmid stress $\tau^{(\alpha)}$ to a strength parameter $g^{(\alpha)}$, termed the slip resistance. The slip resistance increases from an initial value g_0 according to

$$\dot{g}^{(\alpha)} = \sum_{\beta} h_{\alpha\beta}|\dot{\gamma}^{(\beta)}| \tag{3.12}$$

where $h_{\alpha\beta}$ is the so-called hardening matrix.

In the strain gradient crystal plasticity theory, it is assumed that the slip resistance $g^{(\alpha)}$ of a crystallographic system hardens according to

$$\dot{g}^{(\alpha)} = \sum_{\beta} h_{\alpha\beta}\dot{\gamma}_{\mathrm{e}}^{(\beta)} \tag{3.13}$$

where the effective slip rate $\dot{\gamma}_{\mathrm{e}}^{(\alpha)}$ is defined by

$$\dot{\gamma}_{\mathrm{e}}^{(\alpha)} = (|\dot{\gamma}^{(\alpha)}|^{\rho} + |l_{\mathrm{S}}\dot{\gamma}_{\mathrm{S}}^{(\alpha)}|^{\rho} + |l_{\mathrm{T}}\dot{\gamma}_{\mathrm{T}}^{(\alpha)}|^{\rho})^{1/\rho}. \tag{3.14}$$

As discussed by Fleck et al. (1994), $\dot{\gamma}_{\mathrm{S}}^{(\alpha)}$ is the slip gradient in the slip direction and generates hardening via geometrically necessary edge dislocations; likewise, $\dot{\gamma}_{\mathrm{T}}^{(\alpha)}$ is the slip gradient in the transverse direction and gives rise to hardening by geometrically necessary screw dislocations. The exclusion of $\dot{\gamma}_{\mathrm{M}}^{(\alpha)}$ from the hardening relation is motivated by the fact that a slip gradient in the direction of the slip plane normal does not lead to any geometrical necessary dislocations and therefore to no elevated hardening. In relation (3.14), ρ is a parameter describing the interaction between slip rate and slip rate gradient, and in a loose sense it defines the interaction between statistically stored dislocations and geometrically necessary dislocations. The length scales l_{S} and l_{T}, together with l_{M} appearing below, are introduced for dimensional consistency, and have the physical interpretation discussed in the Introduction (Section 2).

The effective slip rate is prescribed by a relation of the form of (3.11),

$$\dot{\gamma}_{\mathrm{e}}^{(\alpha)}/\dot{\gamma}_0 = F(\tau_{\mathrm{e}}^{(\alpha)}/g^{(\alpha)}) \tag{3.15}$$

in which

$$\tau_{\mathrm{e}}^{(\alpha)} = (|\tau^{(\alpha)}|^{\rho} + |_{\mathrm{S}}^{-1}Q_{\mathrm{S}}^{(\alpha)}|^{\rho} + |l_{\mathrm{T}}^{-1}Q_{\mathrm{T}}^{(\alpha)}|^{\rho})^{1/\rho} \tag{3.16}$$

is an effective resolved shear stress. Recall that $\tau^{(\alpha)}$ and $\dot{\gamma}^{(\alpha)}$ are the volume averages of the Schmid stress and slip rate, respectively, at the microscopic level. Furthermore, $\dot{\gamma}_{\mathrm{S}}^{(\alpha)}$ is the volume average of the local gradient of micro slip rate while its work conjugate $Q_{\mathrm{S}}^{(\alpha)}$ is related to the local variation of micro Schmid stress; a similar statement can be made for the work conjugate pairs $(\dot{\gamma}_{\mathrm{T}}^{(\alpha)}, Q_{\mathrm{T}}^{(\alpha)})$ and $(\dot{\gamma}_{\mathrm{M}}^{(\alpha)}, Q_{\mathrm{M}}^{(\alpha)})$. We assume that the slip rate and the local slip rate gradients obey the following proportionality rule of

$$\frac{\dot{\gamma}^{(\alpha)}}{\tau^{(\alpha)}} \equiv \frac{l_{\mathrm{S}}\dot{\gamma}_{\mathrm{S}}^{(\alpha)}}{l_{\mathrm{S}}^{-1}Q_{\mathrm{S}}^{(\alpha)}} \equiv \frac{l_{\mathrm{T}}\dot{\gamma}_{\mathrm{T}}^{(\alpha)}}{l_{\mathrm{T}}^{-1}Q_{\mathrm{T}}^{(\alpha)}} \equiv \frac{l_{\mathrm{M}}\dot{\gamma}_{\mathrm{M}}^{(\alpha)}}{l_{\mathrm{M}}^{-1}Q_{\mathrm{M}}^{(\alpha)}} = \lambda^{(\alpha)} \tag{3.17}$$

where by eqns (3.14) and (3.16)

$$\lambda^{(\alpha)} \equiv \frac{\dot{\gamma}_{\mathrm{e}}^{(\alpha)}}{\tau_{\mathrm{e}}^{(\alpha)}}. \tag{3.18}$$

Equation (3.17) has been proposed by Smyshlyaev and Fleck (1996), but in the sense that $\dot{\gamma}_{\mathrm{S}}^{(\alpha)} \equiv \partial\dot{\gamma}^{(\alpha)}/\partial X_{\mathrm{S}}$ and so on. They considered a rigid-plastic crystal, and obtained a solution for the distribution of slips and slip gradients. However, for an elastoplastic solid, constraints of the type $\dot{\gamma}_{\mathrm{S}}^{(\alpha)} = \partial\dot{\gamma}^{(\alpha)}/\partial X_{\mathrm{S}}$ cannot be satisfied simultaneously with eqn (3.17) for the following reason: these constraints will require a solution for one unknown quantity $\lambda^{(\alpha)}$ to three independent first-order partial differential equations of $s_k^{(\alpha)}\partial(\tau^{(\alpha)}\lambda^{(\alpha)})/\partial X_k = l_{\mathrm{S}}^{-2}Q_{\mathrm{S}}^{(\alpha)}\lambda^{(\alpha)}$, etc. According to the theory of partial differential equations (see Garabedian, 1986 for example), such a solution generally does not exist. In the crystal theory considered by Smyshlyaev and Fleck, $\tau^{(\alpha)}$ and $Q_{\mathrm{S}}^{(\alpha)}$ are also unknowns and they provide additional degrees of freedom so that a solution can be found. In this paper, we get around this difficulty by interpreting $\dot{\gamma}_{\mathrm{S}}^{(\alpha)}$ as the average slip gradient rate at the microscopic level, which is generally different from the macroscopic slip rate gradient $\partial\dot{\gamma}^{(\alpha)}/\partial X_{\mathrm{S}}$. This strategy is analogous to the accepted notion that the total strain in a crystal equals the gradient of the displacement field, but the plastic strain is generally not derivable from a 'plastic' displacement field.

A constitutive law remains to be specified for the evolution of the stress and the double stress. On the micro-scale, the Cauchy stress is related to the elastic strain; therefore, the macro stress $\boldsymbol{\sigma}$, defined as the volume average of the microscopic Cauchy stress, is related to the elastic macro strain $\boldsymbol{\varepsilon}^{\mathrm{e}}$ which is the volume average of the microscopic elastic strain. The double stress $\boldsymbol{\tau}$, related to the local average variation of Cauchy stress on the microscale, is taken to depend on the elastic strain gradient $\boldsymbol{\eta}^{\mathrm{e}}$, which is the volume average of the local elastic strain gradient on the microscale. Therefore, it is assumed that

$$\dot{\sigma}_{ij} = C_{ijkl}\dot{\varepsilon}_{kl}^{\mathrm{e}}, \quad \text{and} \quad \dot{\tau}_{ijk} = l_{\mathrm{e}}^2 C_{ijpq}\dot{\eta}_{pqk}^{\mathrm{e}}. \tag{3.19}$$

Here, l_{e} is an elastic length scale parameter and is related to the size of the microvolume δV as discussed in Section 2. Relations (3.19) and (2.12) imply that $\dot{\tau}_{ijk} = l_{\mathrm{e}}^2\,\partial\dot{\sigma}_{ij}/\partial X_k$ when the deformation is purely elastic. All the computations reported

in this paper were obtained using the above elasticity constitutive law. A more general elastic constitutive law governing the double stress and the elastic strain gradients was proposed by Mindlin (1964) and has been subsequently adopted by Fleck and Hutchinson (1997), based on a unique orthogonal decomposition of the strain gradient tensor $\boldsymbol{\eta}$ introduced by Smyshlyaev and Fleck (1996).

3.3. Specifics of the constitutive law

In the following section, we shall examine the shear deformation of a bicrystal. For the sake of simplicity, we adopt a power-law creep model for the effective slip rate:

$$\dot{\gamma}_{\mathrm{e}}^{(\alpha)} = \dot{\gamma}_0 \left(\frac{\tau_{\mathrm{e}}^{(\alpha)}}{g^{(\alpha)}} \right)^{1/m} \tag{3.20}$$

where the parameter m is the rate-sensitivity index which is generally between zero (the rate-independent limit) and unity. Unless stated otherwise, m is taken to be 0.01 to closely approximate the rate-independent case. In all the computations conducted, the reference slip rate $\dot{\gamma}_0$ serves as a scaling parameter to normalise the applied strain rate. The hardening matrix is given by

$$h_{\alpha\beta} = h\delta_{\alpha\beta} + qh(1-\delta_{\alpha\beta}) \tag{3.21}$$

with the constant $q = 1.4$ as a latent hardening index and $\delta_{\alpha\beta}$ is the Kronecker delta symbol. In general, the self-hardening modulus h can be taken to be a function of the effective slip accumulated over the whole loading history, $\gamma_{\mathrm{e}} = \Sigma_\alpha \int \dot{\gamma}_{\mathrm{e}}^{(\alpha)} \, \mathrm{d}t$. In this paper, we assume linear hardening and set h equal to a constant value h_0. The initial slip resistance is taken to be the same value g_0 for all slip systems and, in the majority of the numerical calculations, h_0 is taken to be 10 times g_0. The elastic modulus C_{ijkl} is taken to be isotropic, with Young's modulus $E = 10^3 \times g_0$ and Poisson's ratio $\nu = 0.25$. The corresponding shear modulus is $G = 400\ g_0$. All constitutive length scales, l_{e}, l_{S}, l_{M} and l_{T}, are assumed to equal a constant value l.

The above rate-dependent strain gradient crystal theory has been implemented within the finite element method framework, for the case of crystals undergoing in-plane deformation. The details of the finite element implementation are presented in Appendix A and the tangent modulus scheme is summarised in Appendix B.

4. Application: Shear of a bicrystal

As an application of the strain gradient crystal plasticity theory, a bicrystal undergoing in-plane shear deformation is studied. As shown schematically in Fig. 2, the bicrystal consists of two single crystal strips infinitely long in the X_1- and X_3-directions and of thickness D in the X_2-direction. It is imagined that the two grains are 'cut' from the same single crystal and are perfectly bonded (no relative displacements) with a mismatch angle in the lattice orientation with respect to the Cartesian co-ordinate system. For the case of uniform slip on a single system of the single crystal, the slip

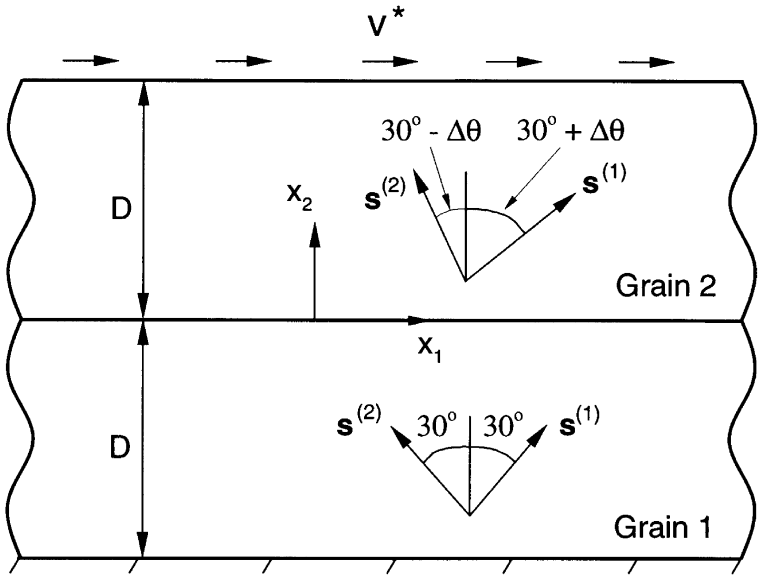

Fig. 2. The geometry and notation of a lamellar bicrystal under plane-strain shear deformation. A uniform velocity v^* in the X_1-direction is prescribed along the top surface. $\mathbf{s}^{(1)}$ and $\mathbf{s}^{(2)}$ are unit vectors in the slip directions of the two planar slip systems at any point.

resistance increases linearly with shear strain, with a hardening modulus h_0 and an initial strength g_0. A Planar-Double-Slip model is considered in this paper (see for example Rashid and Nemat-Nasser, 1992): each grain has two slip systems, and the slip directions and slip plane normals lie in the (X_1, X_2) plane. It is well known that the planar double slip model can mimic the actual plane-strain deformation in a (110) type plane of a face-centred-cubic (FCC) crystal. The two effective slip systems consist of slip directions and slip plane normals lying in the same (110) plane, and give the same overall plastic strain as the 12 slip systems in the FCC crystal. In this paper, we assume that the slip directions in grain 1 are aligned at -30 and 30° from the X_2-axis while those in grain 2 are aligned at angles of $-30^\circ+\Delta\theta$ and $30^\circ+\Delta\theta$ (see Fig. 2).

On the bottom surface of the bicrystal the displacement and the higher order tractions vanish, $u_1 = u_2 \equiv 0$ and $r_1 = r_2 \equiv 0$. On the top face, the higher order tractions again vanish, $r_1 = r_2 \equiv 0$ but a uniform velocity is prescribed along the X_1-direction, $\dot{u}_1 = v^*$, corresponding to an average shear strain rate of $\dot{\bar{\varepsilon}}_{12} = v^*/4D$. Out-of-plane deformation is constrained, $u_3 \equiv 0$.

The choice of higher-order boundary conditions at the interface $X_2 = 0$ plays an important role in determining the deformation state of the bicrystal. If one assumes that the interface places no additional constraint on the deformation field except requiring continuity of displacement and traction t_i, then the higher-order traction r_i vanishes on the interface and the strain gradient theory gives identical results to those of its classical scale-independent counterpart. The deformation state thus predicted is uniform in each grain but discontinuous across the boundary; also, no size-dependence

is predicted for the bicrystal yield strength. If, on the other hand, one assumes that the interface imposes an additional constraint that the normal gradient of displacement is continuous across the grain boundary, then the predicted deformation exhibits a strong grain size-dependence, as detailed below. The rationale of this constraint can only be verified or refuted by well-controlled experiments through which detailed characterisation of deformation (e.g., lattice rotation angle) can be made in a region surrounding the interface and spanning a few tens of microns.

4.1. The nature of the solution

The general structure of the solution is as follows. The solution is one-dimensional in nature: all deformation variables depend on X_2 only. In grain 1 symmetry of the slip orientations dictates the slips are equal, $\gamma^{(1)} = \gamma^{(2)}$. In grain 2, the lattice mismatch $\Delta\theta$ generally implies that $\gamma^{(1)} \neq \gamma^{(2)}$. In both grains, the non-vanishing components of strain and strain gradient are ε_{12} ($\equiv\varepsilon_{21}$), ε_{22}, η_{122} ($\equiv\eta_{212}$) and η_{222}. The tensile stain component ε_{22} and its gradient η_{222} arise from the plastic anisotropy associated with the non-symmetric slips in grain 2 and from the strain gradient effect. At the interface we assume continuity of displacement u_1 and of displacement gradient $\partial u_1/\partial X_2$. This implies that the total shear strain ε_{12} is continuous at the interface, but the slips and lattice rotation can jump in value. Continuity of traction t_1 and of higher-order traction r_1 is also enforced at the interface.

A simple 2-D finite element mesh of forty nine-noded quadrilateral QU34L4 elements (see Appendix A for details about the elements) is used for each grain. Periodic boundary conditions are applied to enforce uniformity of deformation along the X_1-direction: for any two nodes equidistant from the interface the values of the nodal degrees of freedom are identical, and the nodal forces are equal in magnitude but opposite in sign.

4.2. Deformation state in large grains

In this subsection, we investigate the deformation of a thick bicrystal with $D/l = 100$. We present in Fig. 3(a) the distribution of total strain $\varepsilon_{12} = (\partial u_1/\partial X_2)/2$ for the case $\Delta\theta = 30^\circ$ and $\rho = 1$ [recall eqn (3.14)]. The largest difference between the Schmid factors and the plastic deformation in the two grains is attained at $\Delta\theta = 30^\circ$. The maximum Schmid factor in the bicrystal is $\mu_{12} = 0.5$, giving a shear yield strain of the solid $g_0/(4\mu_{12}G) = 0.125\%$; therefore, the strains shown in Fig. 3(a) are deep in the plastic range. It is clear from the figure that the strain is continuous at the grain boundary but has a non-uniform distribution within a narrow boundary layer on each side of the grain boundary. Away from the grain boundary, the strain approaches the conventional crystal theory prediction. Similar boundary layers of slip are evident from the distribution of slip γ on the second slip system, see Fig. 3(b). We do not display results for the first slip system as the slip on this system is negligible within grain 2.

An important measure of the crystal deformation is the rotation of the lattice. The lattice rotation angle ω is defined as the total material rotation minus the material

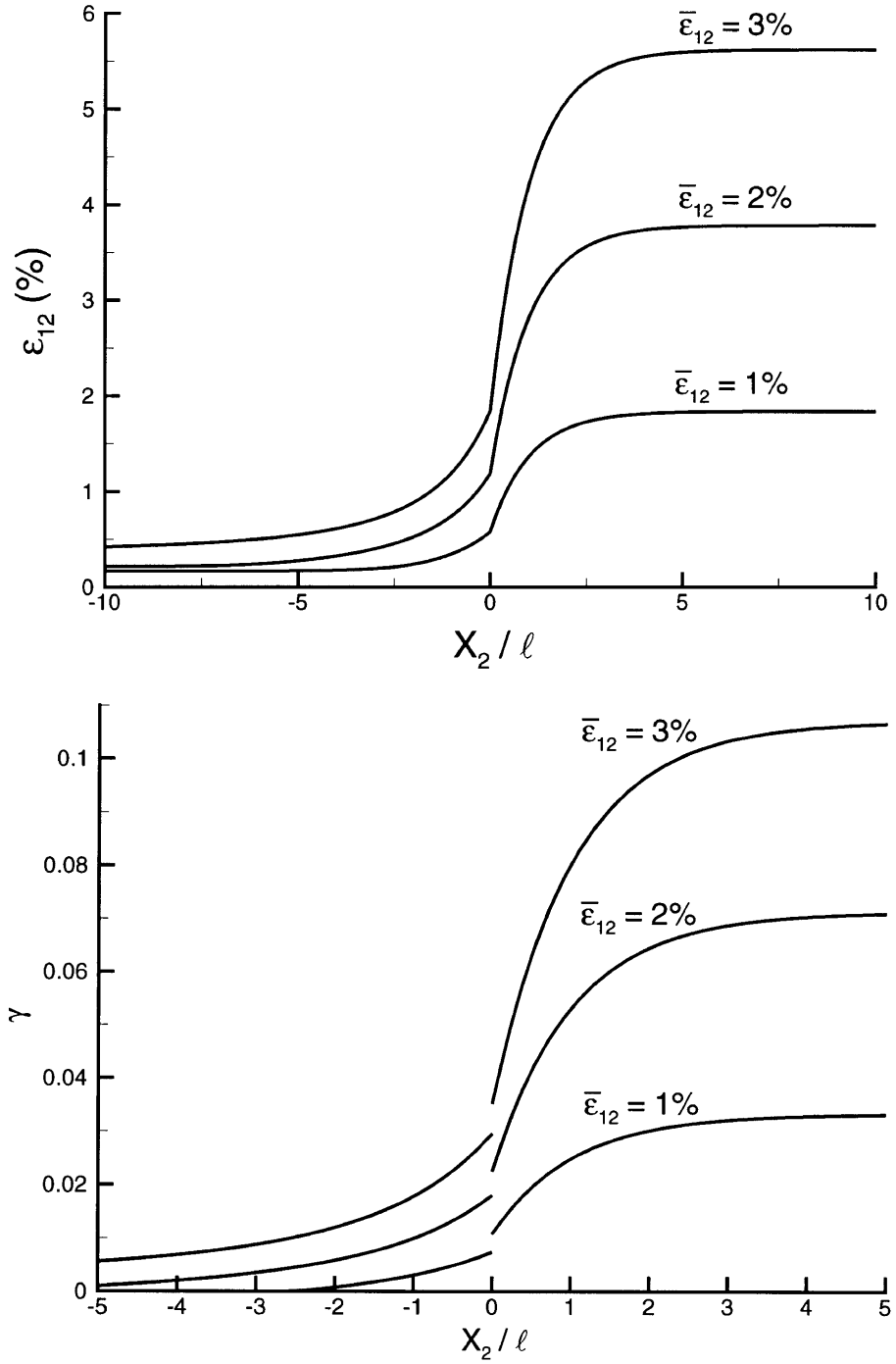

Fig. 3. (a) The distribution of total shear strain ε_{12} along the X_2-direction, normal to the grain boundary; (b) the slip γ on the second slip system in both strains, as a function of X_2. $\Delta\theta = 30^\circ$, $D/l = 100$ and $\rho = 1$.

rotation associated with plastic deformation. On adopting the sign convention of clockwise positive, ω can be written as

$$\omega = \varepsilon_{12} - \sum_{\alpha} \gamma^{(\alpha)}/2 \tag{4.1}$$

and is plotted in Fig. 4 for $\Delta\theta = 30^\circ$. In the calculations, the lattice vectors do not change with time. The effect of finite deformation has not been explored but is not expected to change the overall distribution of ω. The non-linear interaction between strain hardening and strain gradient hardening is addressed by giving results for both $\rho = 1$ and $\rho = 2$: the effect of the magnitude of ρ on lattice rotation is minor. The distribution of lattice rotation also shows the existence of a boundary layer adjacent to the grain boundary; remote from the grain boundary ω asymptotes to the prediction of the classical theory. The jump in lattice rotation ω at the interface is small compared to the classical solution, but remains finite by the following argument. Grain 2 has a larger plastic rotation $\Sigma_\alpha \gamma^{(\alpha)}/2$ than grain 1. At the interface the strain component ε_{12} is continuous. Thus, by (4.1), the lattice rotation at the interface is less in grain 2 than in grain 1.

It is instructive to explore the sensitivity of the boundary layer width to the lattice misorientation $\Delta\theta$. We take as a measure of the boundary layer width the distance

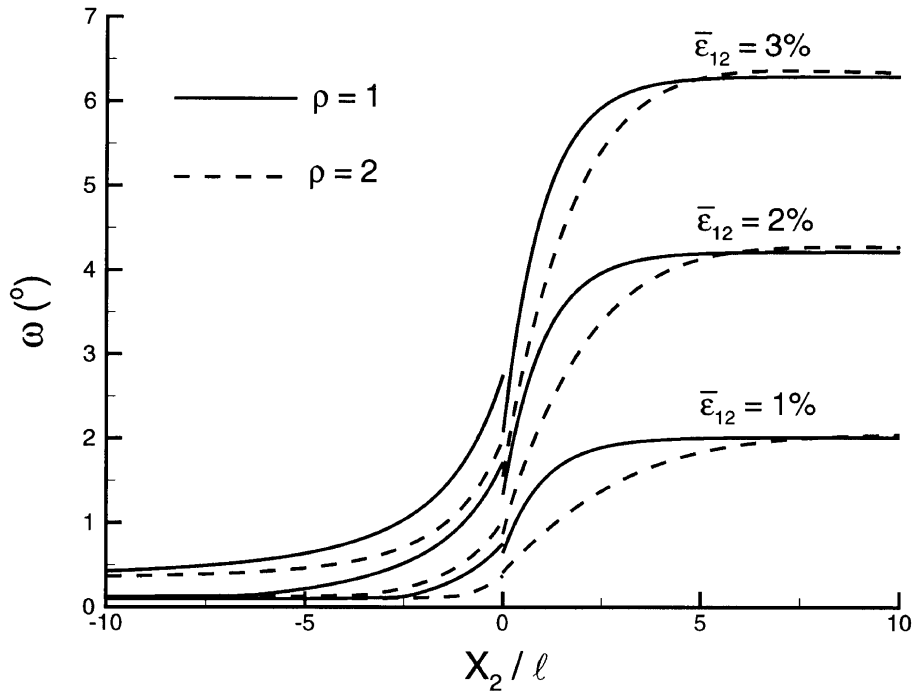

Fig. 4. Lattice rotation angle ω as a function of distance X_2 from the grain boundary, for $\Delta\theta = 30^\circ$. $D/l = 100$.

from the interface over which the lattice rotation deviates by more than 0.2° from the remote value (given by the classical solution, neglecting gradient effects). The widths w_1 and w_2 of the boundary layer in grains 1 and 2, respectively, are plotted in Fig. 5 vs $\Delta\theta$, at an average strain $\bar{\varepsilon}_{12}$ of 3%, with $\rho = 1$. The total width $w = w_1 + w_2$ is included in the figure. The symbols denote individual calculations. The widths as functions of $\Delta\theta$ are mirror symmetric about $\Delta\theta = 90^\circ$ and have a periodicity of $\Delta\theta = 180^\circ$.

The dependence of the widths on the mismatch angle is strong. A peak in all widths is attained at $\Delta\theta = 30^\circ$. This geometric orientation gives a strong gradient effect by the following argument. At this mismatch angle the plastic deformation in grain 2 is predominantly by slip along slip system (2) whose glide direction is aligned with the X_2 direction. This slip system has a Schmid factor of -0.5 and gives rise to a negative plastic rotation (i.e., in the anti-clockwise direction) and thereby to a large lattice rotation ω (see Fig. 4 for the value of ω). Continuity of strain ε_{12} across the interface leads to a large higher-order stress at the interface ($r_1 = 1.33lg_0$) and to a thick boundary layer within both grains.

In contrast, for $\Delta\theta = 60^\circ$, the plastic deformation in grain 2 is by slip on slip system (1), with its slip direction aligned along the direction of remote shear X_1 and with a Schmid factor of 0.5; the grain has a positive plastic spin and by (4.1) a small lattice

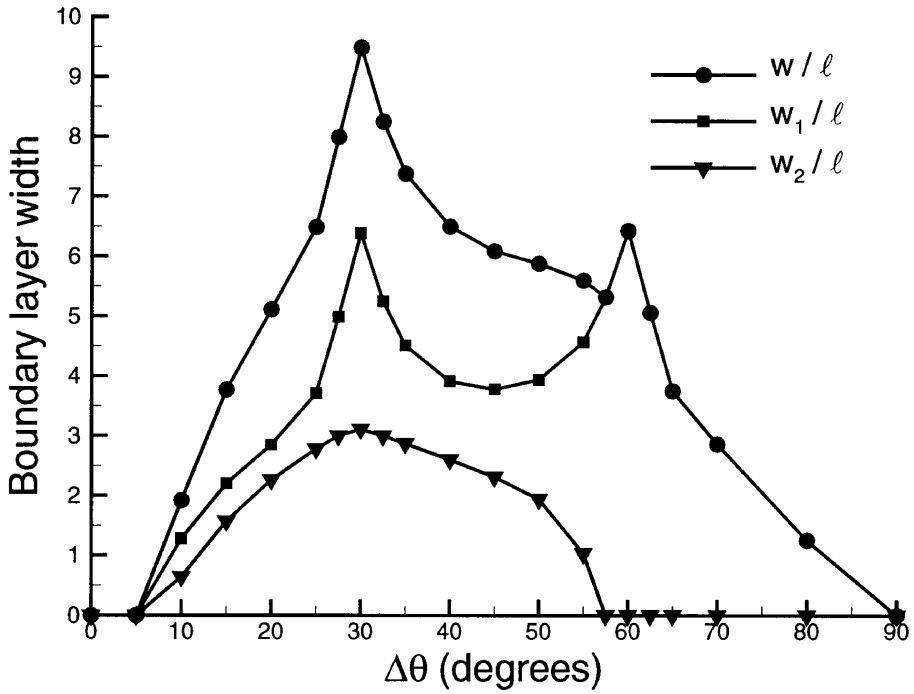

Fig. 5. The boundary layer width at 3% average shear strain $\bar{\varepsilon}_{12}$ as a function of the mismatch angle $\Delta\theta$. The distribution has mirror symmetry about $\Delta\theta = 90^\circ$ and a period of $\Delta\theta = 180^\circ$. $D/l = 100$. $\rho = 1$.

rotation of 0.09–0.15°. Although higher-order stress exists at the interface ($r_1 = 1.26\ lg_0$), the lattice rotation ω in grain 2 is smaller than the chosen cut-off value of 0.2° and the boundary layer width w_2 is taken to vanish. Grain 1 has a larger lattice rotation 0.35–2.61° and the higher-order stress at the interface gives rise to a wide boundary layer.

Figure 5 suggests a systematic set of bicrystal experiments whereby the boundary layer thickness is measured as a function of lattice mismatch angle. Recently, it has become practical to measure lattice rotation adjacent to a grain boundary using the Orientation Imaging Microscope (Adams et al., 1993).

It is interesting to compare the micro slip gradient $\gamma_S^{(2)}$ on slip system (2) with the corresponding macroscopic slip gradient $\gamma_{,S}^{(2)} = s_2^{(2)} \partial \gamma^{(2)} / \partial X_2$, for the case $\Delta\theta = 30°$ and $\rho = 1$. The values of the two slip gradients are plotted vs X_2/l in Fig. 6 at three values of average shear strain $\bar{\varepsilon}_{12}$. The corresponding slip distribution has already been shown in Fig. 3(b). In general, the two gradients agree well and the difference diminishes as $\bar{\varepsilon}_{12}$ increases. For example at $\bar{\varepsilon}_{12} = 3\%$, $\gamma_S^{(2)}$ is about 3% smaller than $\gamma_{,S}^{(2)}$ in grain 1 at the interface while in grain 2, the difference is about 10% at the interface, 5% at the next mesh point and less than 1% at all other points. The generally good agreement is not surprising. Recall that the total strain gradient $\eta_{ijk} = \partial \varepsilon_{ij} / \partial X_k$. As deformation proceeds, the plastic strain ε_{ij}^p and plastic strain gradient η_{ijk}^p increasingly dominate the elastic contribution to the strain and strain gradient, respectively, and η_{ijk}^p converges

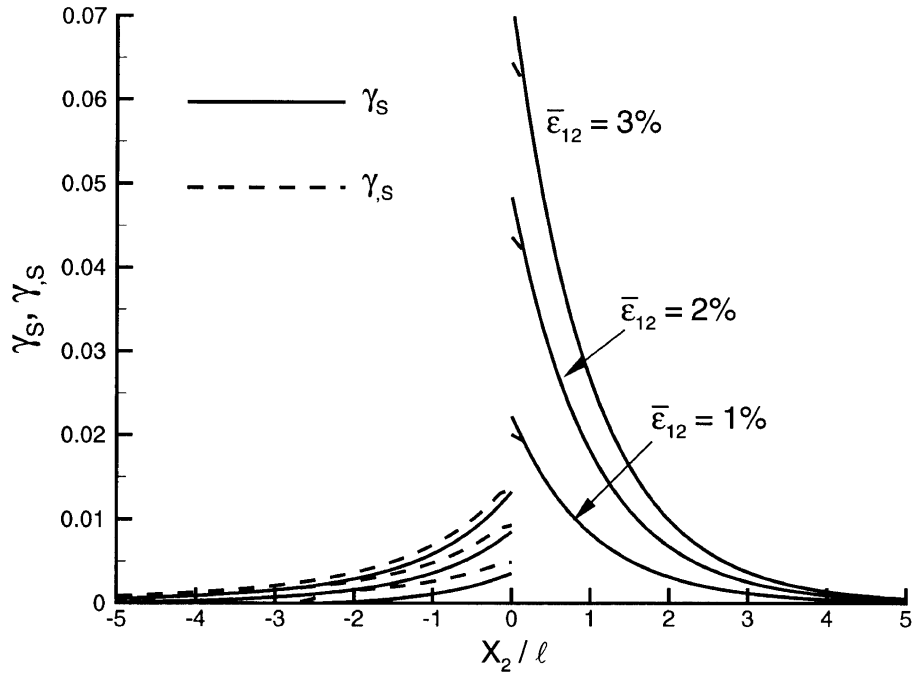

Fig. 6. The micro slip gradient γ_S and the macro slip gradient $\gamma_{,S}$ as a function of distance X_2 from the grain boundary, for $D/l = 100$. $\Delta\theta = 30°$ and $\rho = 1$. The gradients are associated with the second slip system.

to $\partial\varepsilon^{\mathrm{p}}_{ij}/\partial X_k$. In grain 2, only slip system (2) is active and its orientation renders $\gamma^{(2)}_{\mathrm{M}} = \gamma^{(2)}_{,\mathrm{M}} = 0$, thereby $\eta^{\mathrm{p}}_{122} = \mu^{(2)}_{12}s^{(2)}_{2}\gamma^{(2)}_{\mathrm{S}}$ and $\varepsilon^{\mathrm{p}}_{12,2} = \mu^{(2)}_{12}s^{(2)}_{2}\gamma^{(2)}_{,\mathrm{S}}$. Thus, $\gamma^{(2)}_{\mathrm{S}}$ converges to $\gamma^{(2)}_{,\mathrm{S}}$, as shown in the figure. In grain 1, the slips on the two systems are equal, with $\eta^{\mathrm{p}}_{122} = 2\mu^{(2)}{}_{12}\mathrm{s}^{(2)}{}_{2}\gamma^{(2)}{}_{\mathrm{s}}$ and $\varepsilon^{\mathrm{p}}_{12,2} = 2\mu^{(2)}_{12}s^{(2)}_{2}\gamma^{(2)}_{,\mathrm{S}}$. Therefore, $\gamma^{(2)}_{\mathrm{S}}$ and $\gamma^{(2)}_{,\mathrm{S}}$ converge as η^{p}_{122} converges to $\varepsilon^{\mathrm{p}}_{12,2}$. The relatively poor agreement in grain 2 near the interface is due to the numerical differentiation used to estimate $\gamma^{(2)}_{,\mathrm{S}}$ near the boundary.

4.3. Deformation state in small grains

As reported above, for bicrystals with a large grain size $D \gg l$, the gradient theory predicts a deformation field identical to that of the classical crystal theory except in a narrow boundary layer adjacent to the grain boundary. It is also of interest to compare the two theories for the case of D comparable in value to l. Recall that the classical theory lacks a constitutive length scale, so the predicted deformation state is independent of the magnitude of D. We shall demonstrate that the strain gradient theory predicts significant change in deformation state with diminishing grain size. Consider a bicrystal with a grain size $D = l$. The lattice rotation angle ω is plotted against X_2/l in Fig. 7, for $\Delta\theta = 30^\circ$ and for selected values of $\bar{\varepsilon}_{12}$ and ρ. The deformation is non-uniform throughout the bicrystal, and the lattice rotation is dramatically different from that predicted by the classical theory, as given by the asymptotes in Fig. 4.

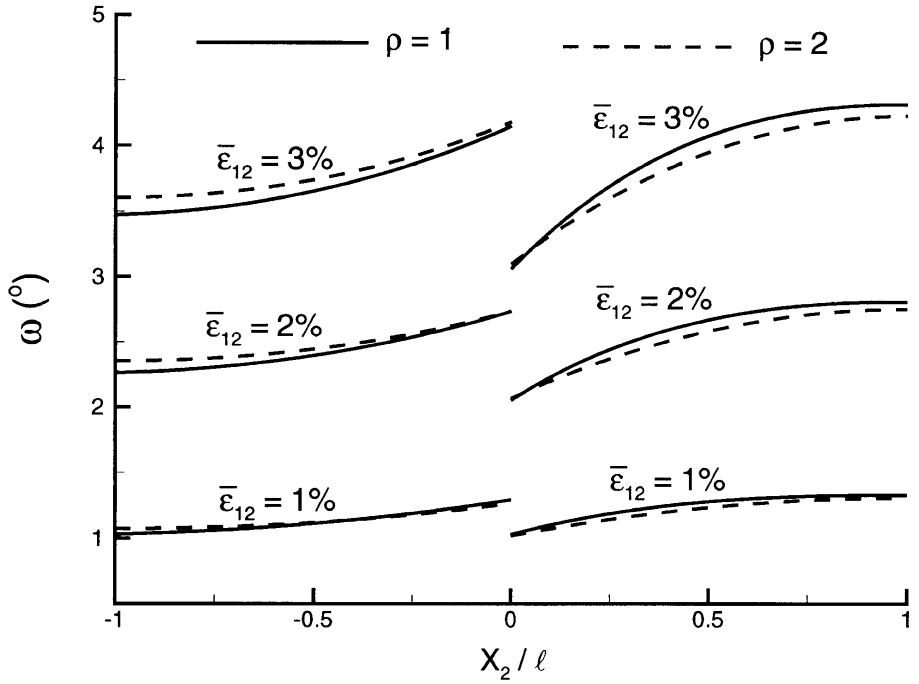

Fig. 7. Lattice rotation angle ω as a function of distance X_2 from the grain boundary for $D/l = 1$. $\Delta\theta = 30^\circ$.

Overall, the gradient theory smooths out the difference in lattice rotation of the two grains, except in the vicinity of the grain boundary. There is a cross-over of the lattice rotation, in a region of a width of about 0.2 l adjacent to the interface, for the reason already discussed in relation to Fig. 4.

4.4. Grain-size dependence of bicrystal yield strength

It is well-known that the yield strength, denoted by τ_Y, of a polycrystal obeys a Hall–Petch relation (Hall, 1951; Petch, 1953):

$$\tau_Y \approx \tau_0 + \kappa D^{-1/2} \tag{4.2}$$

where τ_0 and κ are material constants, and D is the average grain size. Conventional crystal plasticity theory is unable to predict the Hall–Petch effect. The grain size-dependence of the overall yield strength of the bicrystal is studied using the current strain gradient crystal theory. In results reported below, unless otherwise stated, the 'yield strength' τ_Y is chosen to be the surface traction per unit area at 0.1% plastic average strain $\bar{\varepsilon}^p_{12}$. We report below predictions of the grain size effect as a function of lattice orientation mismatch $\Delta\theta$ and hardening modulus h_0.

4.5. (i) Effect of orientation mismatch angle

Figure 8 shows the relation between the surface traction per unit area t_1 and the average shear strain for various relative grain size D/l. In the figure, two values of the

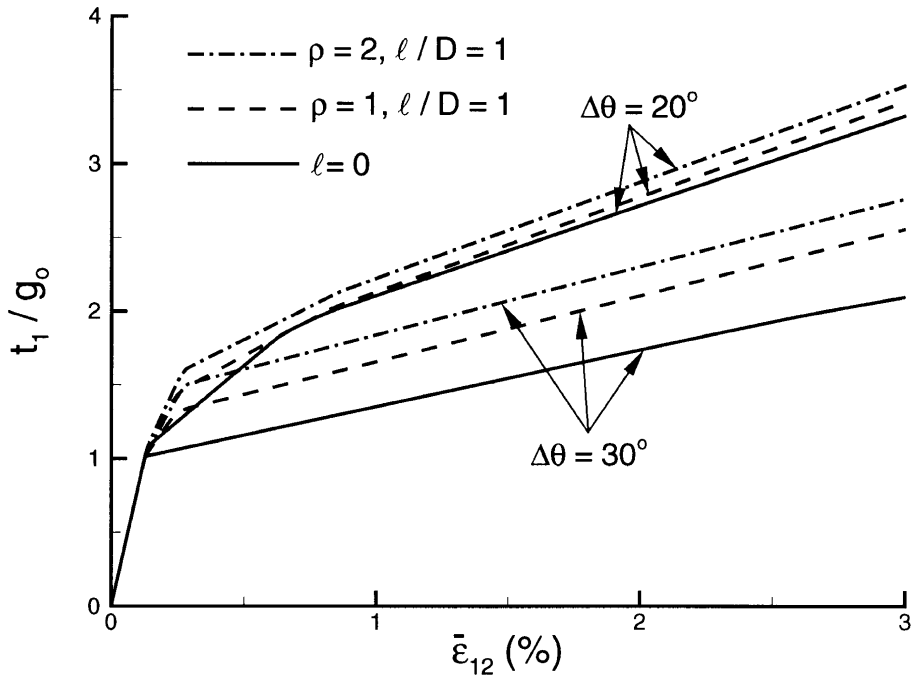

Fig. 8. The surface traction t_1 vs the average strain $\bar{\varepsilon}_{12}$ for various grain sizes D/l.

mismatch angle are chosen: $\Delta\theta = 20^\circ$ and $\Delta\theta = 30^\circ$. There is a considerable size effect, the magnitude of which is rather insensitive to the choice of the offset yield strain. It is further seen from Fig. 8 that the coupling between the slip and slip gradients characterised by the index ρ has a considerable effect on the grain size dependence. Generally, a linear coupling ($\rho = 1$) leads to a smaller grain size effect on the yield strength than quadratic coupling ($\rho = 2$). The 0.1% offset yield strength τ_Y is plotted against grain size D in Fig. 9 for various lattice mismatches. The grain size effect is strong for $0.3 < (l/D)^{1/2} < 1$, that is for $l < D < 10\,l$.

The classical theory prediction of the yield strength τ_0 is plotted against the mismatch angle $\Delta\theta$ in Fig. 10(a). The calculated strength as a function of $\Delta\theta$ is mirror-symmetric about $\Delta\theta = 90^\circ$ and has a periodicity of $\Delta\theta = 180^\circ$. An identical shear yield strength is predicted at mismatch angles of 30 and 60° for the following reason. In grain 2 the Schmid factors for the two slip systems have identical absolute values at $\Delta\theta = 30^\circ$ and at $\Delta\theta = 60^\circ$ and hence the bicrystal undergoes the same strain state.

Now return to the predictions of the strain gradient theory. The elevation in flow strength associated with the grain size effect ($\tau_Y - \tau_0$) is plotted against the mismatch angle $\Delta\theta$ in Fig. 10(b), for $l/D = 1$. The solid lines correspond to the strength elevation at 0.1% offset strain while the dashed lines are for 1% offset strain. The calculated strength is again mirror-symmetric about $\Delta\theta = 90^\circ$ and has a periodicity $\Delta\theta = 180^\circ$. At $\Delta\theta = 0$, 90 and 180°, there is no mismatch in Schmid factors between grains, no

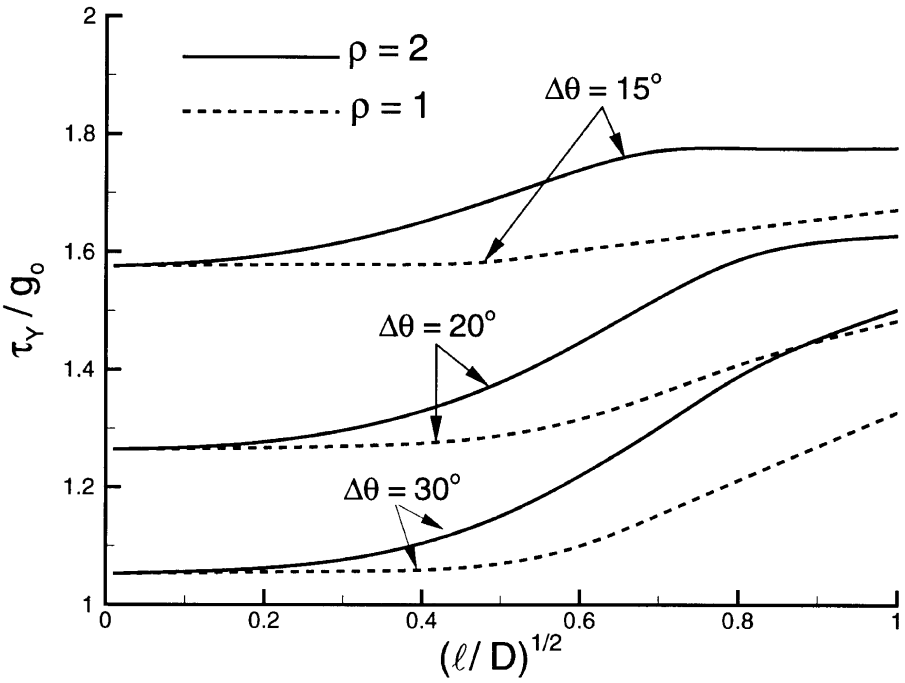

Fig. 9. The effect of mismatch angle on the grain size dependence of yield strength of the bicrystal.

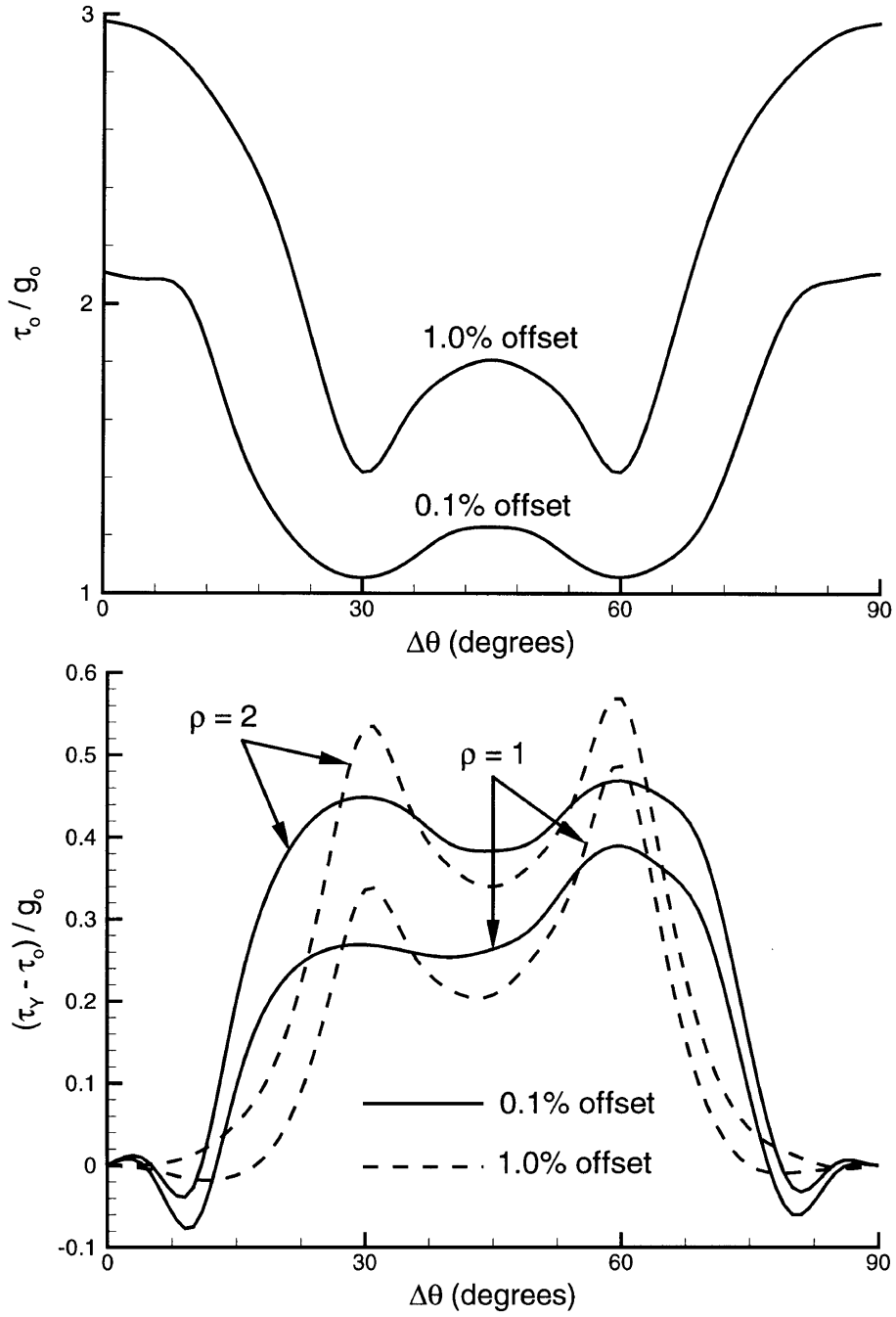

Fig. 10. (a) The classical theory prediction of the bicrystal yield strength τ_0 as a function of the mismatch angle $\Delta\theta$; (b) $\tau_Y - \tau_0$ as a function of the mismatch angle $\Delta\theta$. τ_Y is calculated using the strain gradient theory for $l/D = 1$.

strain gradients and therefore no grain size dependence. For other mismatch angles, the strain gradient crystal formulation suggests a significant grain size effect.

It is further noted from Figs. 10(a) and (b) that the strain gradient theory predicts a slightly lower yield strength τ_Y for $\Delta\theta = 30^\circ$ than for $\Delta\theta = 60^\circ$. Yet, the effective shear stress on the dominant slip system is greater for $\Delta\theta = 30^\circ$ than for $\Delta\theta = 60^\circ$: this can be traced back to the different roles that γ_S and γ_M play in the hardening relation (3.14). At $\Delta\theta = 30^\circ$, slip system (2) in grain 2 is dominant and the finite slip gradient $\gamma_S^{(2)}$ contributes to the hardening, while at $\Delta\theta = 60^\circ$ the slip system (1) is dominant in grain 2 and has a slip gradient $\gamma_M^{(1)}$ which does not lead to elevated hardening. Thus, the effective resolved stress $\tau_e^{(2)}$ at $\Delta\theta = 30^\circ$ is larger than $\tau_e^{(1)}$ at $\Delta\theta = 60^\circ$.

It is clear from Fig. 10(b) that although the precise value of $(\tau_Y - \tau_0)$ at 1% offset is changed by a moderate amount from the corresponding value at 0.1% offset, the grain size effect is generally maintained deep into plastic range. This indicates that the grain size effect is not intrinsically an elastic–plastic effect.

4.6. (*ii*) *Effect of the self-hardening modulus*

To study the effect of the self-hardening modulus h_0 on the grain size effect, computations have been carried out for various h_0, at a fixed mismatch angle $\Delta\theta = 30^\circ$. The yield strength τ_Y is plotted in Fig. 11(a) and the strength elevation $(\tau_Y - \tau_0)$ is plotted in Fig. 11(b) vs the inverse square root of the relative grain size $(D/l)^{-1/2}$. As expected, the elevation of h_0 leads to a significant increase in yield strength; however, the grain size effect in strength has only a minor dependence on the precise choice of hardening modulus. This is fully consistent with the approach we have adopted: we have sought to give an underlying micromechanical basis to the grain size effect on yield strength, rather than predict a grain size effect based on strain hardening rate.

5. Concluding remarks

Based on the physical argument of elevated hardening due to geometrically necessary dislocations, an elastic–viscoplastic strain gradient crystal plasticity formulation is presented. It fits within the Fleck–Hutchinson strain gradient plasticity theory framework and contains constitutive length scales. The formulation is applied to study the plane strain deformation of a lamellar bicrystal. The choice of interface constraints plays a critical role in affecting the predictions. The weak constraint of displacement continuity gives scale-independent predictions identical to those of classical theories, while the stronger constraint of continuous displacement and continuous total strain leads to a grain size dependence of strength. The classical theory and the gradient theory give almost identical predictions away from the interface but differ significantly within a boundary layer adjacent to the interface.

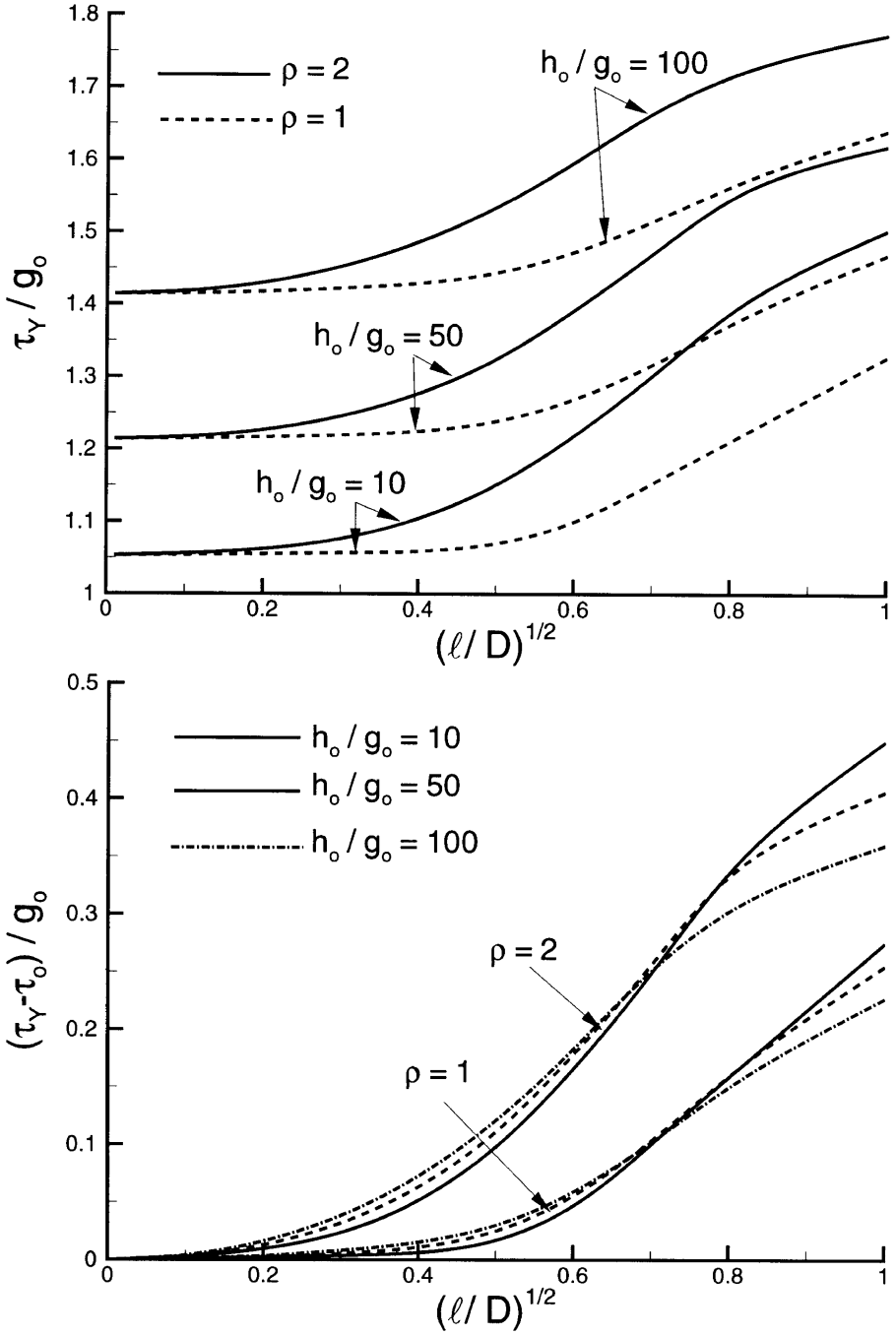

Fig. 11. The effect of the self-hardening modulus on the grain size dependence of the bicrystal yield strength. $\Delta\theta = 30^\circ$. (a) τ_Y vs $(D/l)^{-1/2}$; (b) $\tau_Y - \tau_0$ vs $(D/l)^{-1/2}$.

Acknowledgements

J.Y.S. acknowledges the support by the U.S. Department of Energy and the Lawrence Livermore National Laboratory under contract W-7405-Eng-48. This work is part of a multi-scale modelling project, under the leadership of Drs W. E. King and D. H. Lassila. Helpful discussions with Prof. J. W. Hutchinson and Dr V. P. Smyshlyaev are gratefully acknowledged. The authors would also like to thank the reviewers for their very useful comments.

Appendix A: Finite element implementation of strain gradient crystal theory

The Fleck and Hutchinson (1997) framework of strain gradient plasticity has been implemented in a finite element method code. The details of the implementation are documented in Shu et al. (1998). Only the main implementation details are repeated here. As described in Section 3, the principle of virtual work for the strain gradient theory involves second-order spatial derivatives of displacement or velocity. C^1-continuity of the shape functions for displacement interpolation is necessary if a pure displacement-based formulation of the finite element method is used. There is a reliable rectangular C^1 continuous element (Zienkiewicz and Taylor, 1994) but its shape is a strong limitation. Experimentation with Specht's (1985) triangular plate bending element is not encouraging (Xia and Hutchinson, 1996). Shu et al. (1998) have therefore developed a number of elements based on classical C^0 continuous shape functions by making use of appropriate Lagrange multipliers.

To proceed, let us introduce a second-order tensor $\boldsymbol{\eta}$ which will be forced by a Lagrange multiplier to approximate the displacement gradient within each element. Then, the strain gradient is approximated by the third-order tensor $\hat{\boldsymbol{\phi}}$, defined by

$$\hat{\eta}_{ijk} \equiv \frac{1}{2}\left(\frac{\partial \phi_{ij}}{\partial X_k} + \frac{\partial \phi_{ji}}{\partial X_k}\right). \tag{A.1}$$

For a stress field $\boldsymbol{\sigma}$ and double stress field $\boldsymbol{\tau}$ satisfying the equilibrium relations (3.8)–(3.10), it follows from the divergence theorem that

$$\int_V [\sigma_{ij}\delta\varepsilon_{ij} + \tau_{ijk}\delta\hat{\eta}_{ijk} + \lambda_{ij}(\delta\hat{\varepsilon}_{ij} - \delta\varepsilon_{ij})]\,\mathrm{d}V = \int_s [t_i\delta u_i + n_j r_i \delta\phi_{ji}]\,\mathrm{d}S + \int_s (n_k\tau_{ijk} - n_j r_i)(\delta\phi_{ji} - \delta u_{i,j})\,\mathrm{d}S \tag{A.2}$$

in which $\lambda_{ij} \equiv \tau_{ijk,k}$ and $\hat{\varepsilon}_{ij} = (\phi_{ij} + \phi_{ji})/2$. Here, t_i is the surface traction per unit area and r_i the surface double stress traction per unit area, as defined in eqns (3.9) and (3.10), respectively. If ϕ_{ij} were strictly subjected to the constraint

$$\phi_{ij} = u_{j,i} \tag{A.3}$$

throughout the specimen, then $\hat{\varepsilon}_{ij}$ would become the strain ε_{ij}, $\hat{\eta}_{ijk}$ would become the

strain gradient $\eta_{ijk} \equiv \partial \varepsilon_{ij}/\partial X_k$ and (A.2) would degenerate to the principle of virtual work eqn (3.7). However, strict enforcement of (A.3) would demand elements of C^1-continuity.

To use C^0-continuous shape functions, the kinematic constraint (A.3) is enforced in the following weighted-residual manner via the Lagrange multipliers λ_{ij}:

$$\int_v (\phi_{ji} - u_{i,j}) \delta \lambda_{ij} \, \mathrm{d}V = 0. \tag{A.4}$$

For this reason, ϕ_{ij} is referred to as a relaxed displacement gradient and $\hat{\varepsilon}_{ij}$ as a relaxed strain. By satisfying the constraint (A.3) strictly over the surface where the displacement gradient is prescribed, (A.2) can be rewritten as

$$\int_V [\sigma_{ij} \delta \varepsilon_{ij} + \tau_{ijk} \delta \hat{\eta}_{ijk} + \lambda_{ij} (\delta \hat{\varepsilon}_{ij} - \delta \varepsilon_{ij})] \, \mathrm{d}V \approx \int_s [t_i \delta u_i + n_j r_i \delta \phi_{ji}] \, \mathrm{d}S \tag{A.5}$$

without introducing a significant error. Relations (A.4) and (A.5) constitute the basis of the finite element implementation of the strain gradient theory, using displacement and the relaxed displacement derivatives as independent nodal degrees of freedom. Since only first order derivatives of nodal degrees of freedom are involved, C^0-continuous interpolation of the nodal quantities are sufficient to ensure convergence of the finite element procedure with suitable mesh refinement. For a crystal undergoing small straining, the modifications of (A.4) and (A.5) to rate form is straightforward.

Shu et al. (1998) developed a series of C^0-elements and conducted a comprehensive comparison of their relative performance. The computations reported in this paper made use of the optimal elements, designated QU34L4. These elements are nine-noded isoparametric quadrilaterals. There are two degrees-of-freedom (u_1, u_2) at each node; in addition, at each corner node, there are four additional degrees-of-freedom $(\phi_{11}, \phi_{21}, \phi_{12}, \phi_{22})$. The displacement field is interpolated using standard C^0-quadratic shape functions while the relaxed displacement derivatives are interpolated using conventional bilinear shape functions. The total number of degrees-of-freedom per element is 34. The four Lagrangian multipliers λ_{ij} are assumed to be uniform within each element. A full integration scheme is used: the stress and the double stress terms in the principle of virtual work are integrated by 3×3 Gauss quadrature while the Lagrangian multiplier terms are integrated using 2×2 quadrature.

Appendix B: Rate-tangent modulus for the strain gradient crystal

In this appendix, the 'rate-tangent modulus' scheme of Peirce et al. (1984) is used to derive an elastic–plastic forward gradient modulus relating the increments of stress and double stress to those of strain and strain gradient. The general three-dimensional case is considered.

Recall that the effective slip rate is given by the power-law creep relation (3.20). Following Peirce et al. (1984), the increment of the effective slip on a slip system (α) over a time step Δt is approximated by

$$\Delta\gamma_e^{(\alpha)} = \Delta t((1-\vartheta)\dot{\gamma}_e^{(\alpha)}|_t + \vartheta\dot{\gamma}_e^{(\alpha)}|_{t+\Delta t}) \tag{B.1}$$

where a subscript after a vertical bar is used to denote the time at which the effective slip rate is evaluated. The parameter ϑ ranges from 0–1, with $\vartheta = 0$ corresponding to a simple forward Euler time integration scheme while $\vartheta = 1$ represents backward integration. For simplicity of notation, we shall henceforth omit the use of a subscript t following a vertical bar in denoting any quantities evaluated at time t. A first order Taylor expansion about the current state is used to approximate the effective slip rate at $t+\Delta t$:

$$\dot{\gamma}_e^{(\alpha)}|_{t+\Delta t} = \dot{\gamma}_e^{(\alpha)} + \dot{\gamma}_e^{(\alpha)}\frac{1}{m}\left(\frac{\Delta\tau_e^{(\alpha)}}{\tau_e^{(\alpha)}} - \frac{\Delta g^{(\alpha)}}{g^{(\alpha)}}\right). \tag{B.2}$$

The increment of slip resistance $\Delta g^{(\alpha)}$ follows from the hardening law (3.13) as

$$\Delta g^{(\alpha)} = \sum_\beta h_{\alpha\beta}\Delta\gamma_e^{(\beta)}, \tag{B.3}$$

Substitution of (B.2) and (B.3) into (B.1) leads to

$$\sum_\beta\left[\delta_{\alpha\beta} + \xi^{(\alpha)}\frac{h_{\alpha\beta}}{g^{(\alpha)}}\right]\Delta\gamma_e^{(\beta)} = \dot{\gamma}_e^{(\alpha)}\Delta t + \xi^{(\alpha)}\Delta\tau_e^{(\alpha)} \tag{B.4}$$

in which

$$\xi^{(\alpha)} \equiv \vartheta\frac{\dot{\gamma}_e^{(\alpha)}\Delta t}{m\tau_e^{(\alpha)}}. \tag{B.5}$$

In order to relate the increment of effective slip to the strain and strain gradient increment, we first need to determine the effective resolved shear stress increment $\Delta\tau_e^{(\alpha)}$ in (B.4).

Upon differentiating eqn (3.16), an increment in the effective resolved shear stress is related to the increments of the resolved shear stress and double stresses by

$$\Delta\tau_e^{(\alpha)} = \mathbf{B}^{(\alpha)}(\Delta\tau^{(\alpha)}, \Delta Q_S^{(\alpha)}, \Delta Q_T^{(\alpha)})^T \tag{B.6}$$

in which the components of the vector $\mathbf{B}^{(\alpha)}$ are

$$B_1^{(\alpha)} = \mathrm{sgn}\,(\tau^{(\alpha)})\left|\frac{\tau^{(\alpha)}}{\tau_e^{(\alpha)}}\right|^{\rho-1}, \quad B_2^{(\alpha)} = \mathrm{sgn}\,(l_S^{-1}Q_S^{(\alpha)})\left|\frac{l_S^{-1}Q_S^{(\alpha)}}{\tau_e^{(\alpha)}}\right|^{\rho-1},$$

$$B_3^{(\alpha)} = \mathrm{sgn}\,(l_T^{-1}Q_T^{(\alpha)})\left|\frac{l_T^{-1}Q_T^{(\alpha)}}{\tau_e^{(\alpha)}}\right|^{\rho-1}. \tag{B.7}$$

Here, a superscript T denotes transpose. By virtue of eqns (3.5) and (3.6), (B.6) can be rewritten as

$$\Delta\tau_e^{(\alpha)} = B_1^{(\alpha)}\boldsymbol{\mu}^{(\alpha)} : \Delta\boldsymbol{\sigma} + (B_2^{(\alpha)}\boldsymbol{\psi}_S^{(\alpha)} + B_3^{(\alpha)}\boldsymbol{\psi}_T^{(\alpha)}) \vdots \Delta\boldsymbol{\tau} \tag{B.8}$$

or, in vector form, as

$$\Delta\tau_e^{(\alpha)} = \tilde{\mathbf{P}}^{(\alpha)^T}\Delta\boldsymbol{\Sigma} \tag{B.9}$$

where the vector $\boldsymbol{\Sigma}$ consists of the six components of stress tensor $\boldsymbol{\sigma}$ and the 18 components of the double stress tensor $\boldsymbol{\tau}$. The components of the vector $\tilde{\mathbf{P}}^{(\alpha)}$ can be easily constructed. It remains to express $\Delta\boldsymbol{\Sigma}$ in terms of $\Delta\gamma_e^{(\alpha)}$ before substituting (B.9) into (B.4).

The proportionality rule (3.13) and (3.14) dictate that the slip and micro slip gradient increments after Δt are given by

$$(\Delta\gamma^{(\alpha)}, \Delta\gamma_S^{(\alpha)}, \Delta\gamma_T^{(\alpha)}, \Delta\gamma_M^{(\alpha)})^T = \mathbf{A}^{(\alpha)}\Delta\gamma_e^{(\alpha)} \tag{B.10}$$

where the components of the vector $\mathbf{A}^{(\alpha)}$ are

$$A_1^{(\alpha)} \equiv \frac{\tau^{(\alpha)}}{\tau_e^{(\alpha)}}, \quad A_2^{(\alpha)} \equiv \frac{Q_S^{(\alpha)}}{l_S^2\tau_e^{(\alpha)}}, \quad A_3^{(\alpha)} = \frac{Q_T^{(\alpha)}}{l_T^2\tau_e^{(\alpha)}}, \quad A_4^{(\alpha)} = \frac{q_M^{(\alpha)}}{l_M^2\tau_e^{(\alpha)}}. \tag{B.11}$$

The overall plastic strain increment is given by

$$\Delta\boldsymbol{\varepsilon}^p = \sum_\alpha A_1^{(\alpha)}\boldsymbol{\mu}^{(\alpha)}\Delta\gamma_e^{(\alpha)} \tag{B.12}$$

and the plastic strain gradient increment is given by

$$\Delta\boldsymbol{\eta}^p = \sum_\alpha (A_2^{(\alpha)}\boldsymbol{\psi}_S^{(\alpha)} + A_3^{(\alpha)}\boldsymbol{\psi}_T^{(\alpha)} + A_4^{(\alpha)}\boldsymbol{\psi}_M^{(\alpha)})\Delta\gamma_e^{(\alpha)}. \tag{B.13}$$

For later convenience of notation, (B.12) and (B.13) are combined in vector form as

$$\Delta\mathbf{E}^p = \sum_\alpha \mathbf{P}^{(\alpha)}\Delta\gamma_e^{(\alpha)} \tag{B.14}$$

where the vector $\Delta\mathbf{E}$ contains all the components of strain and strain gradient increments. The vector $\mathbf{P}^{(\alpha)}$ can be constructed in a straightforward fashion and is not listed here. The linear elastic constitutive law (3.19) is rewritten in vector form, upon making use of (B.14), to obtain

$$\Delta\boldsymbol{\Sigma} = \tilde{\mathbf{C}}(\Delta\mathbf{E} - \Delta\mathbf{E}^p) = \tilde{\mathbf{C}}\Delta\mathbf{E} - \sum_\alpha \tilde{\mathbf{C}}\mathbf{P}^{(\alpha)}\Delta\gamma_e^{(\alpha)}. \tag{B.15}$$

Here, $\tilde{\mathbf{C}}$ denotes the overall elastic modulus matrix and can be constructed from (3.19).

Upon making use of (B.15), we can now proceed to substitute (B.9) into (B.4) and thereby eliminate $\Delta\tau_e^{(\alpha)}$ to get

$$\sum_\beta N_{\alpha\beta}\Delta\gamma_e^{(\beta)} = \dot{\gamma}_e^{(\alpha)}\Delta t + \xi^{(\alpha)}\tilde{\mathbf{P}}^{(\alpha)^T}\tilde{\mathbf{C}}\Delta\mathbf{E} \tag{B.16}$$

in which

$$N_{\alpha\beta} = \delta_{\alpha\beta} + \xi^{(\alpha)} \left(\frac{h_{\alpha\beta}}{g^{(\alpha)}} + \frac{\tilde{\mathbf{P}}^{(\alpha)\mathrm{T}} \tilde{\mathbf{C}} \mathbf{P}^{(\beta)}}{\tau_{\mathrm{e}}^{(\alpha)}} \right) \tag{B.17}$$

eqn (B.16) is inverted to obtain the effective slip increments

$$\Delta\gamma_{\mathrm{e}}^{(\alpha)} = \sum_{\beta} N_{\alpha\beta}^{-1} \left[\dot{\gamma}_{\mathrm{e}}^{(\beta)} \Delta t + \xi^{(\beta)} \tilde{\mathbf{P}}^{(\beta)\mathrm{T}} \tilde{\mathbf{C}} \Delta \mathbf{E} \right] \tag{B.18}$$

where the superscript -1 denotes the inverse. Finally, upon substituting (B.18) into (B.15), one obtains the following governing relation between stress and strain increments:

$$\Delta\boldsymbol{\Sigma} = \left\{ \tilde{\mathbf{C}} - \sum_{\alpha} \sum_{\beta} \xi^{(\beta)} \tilde{\mathbf{C}} \mathbf{P}^{(\alpha)} N_{\alpha\beta}^{-1} \tilde{\mathbf{P}}^{(\beta)\mathrm{T}} \tilde{\mathbf{C}} \right\} \Delta\mathbf{E} - \sum_{\alpha} \sum_{\beta} \tilde{\mathbf{C}} \mathbf{P}^{(\alpha)} N_{\alpha\beta}^{-1} \dot{\gamma}_{\mathrm{e}}^{(\beta)} \Delta t. \tag{B.19}$$

The first term in brackets on the right-hand side of (B.19) is the rate tangent modulus.

References

Acharya, A., Bassani, J.L., 1995. On non-local flow theories that preserve the classical structure of incremental boundary value problems. In: Micromechanics of Plasticity and Damage of Multiphase Materials. IUTAM Symposium, Paris, 29 August–1 September.

Adams, B.L., Wright, S.I., Kunze, K., 1993. Orientation imaging: the emergence of a new microscopy. Metall. Trans. 24A, 819.

Aifantis, E.C., 1984. On the microstructural origin of certain inelastic models. Trans. ASME J. Engng Mater. Tech. 106, 326–330.

Ashby M.F., 1970. The deformation of plastically non-homogeneous alloys. Phil. Mag. 21, 399–424.

Begley, M.R., Hutchinson, J.W., 1997. The mechanics of size-dependent indentation. Harvard University Report Mech-309, July.

Cosserat, E., Cosserat, F., 1909. Theorie des Corps Deformables. Hermann et Fils, Paris.

Fleck, N.A., Hutchinson, J.W., 1993. A phenomenological theory for strain gradient effects in plasticity. J. Mech. Phys. Solids 41, 1825–1857.

Fleck, N.A., Muller, G.M., Ashby, M.F., Hutchinson, J.W., 1994. Strain gradient effects in plasticity: theory and experiment. Acta Metall. 42, 475–487.

Fleck, N.A., Hutchinson, J.W., 1997. Strain gradient plasticity. In: Adv. Appl. Mech. 33, 295–362.

Forest, S., Cailletaud, G., 1995. Strain localisation in single crystals: bifurcation analysis, effects of boundaries and interfaces. Eur. J. Mech., A/Solids 14, 747–771.

Garabedian, P.R., 1986. Partial Differential Equations, 2nd ed. Chelsea Pub. Co., New York.

Hall, E.O., 1951. The deformation and ageing of mild steel. Proc. Phys. Soc. B64, 747–753.

Kubin, L.P., Canova, G., Condat, M., Devincre, B., Pontikis, V., Brechet, Y., 1992. In: Martin, G., Kubin, L.P. (Eds.), Non-linear Phenomena in Materials Science II. Sci-Tech, Vaduz.

Mindlin, R.D., 1964. Micro-structure in linear elasticity. Archive Rational Mechanics Analysis 16, 51–78.

Peirce, D., Asaro, R.J., Needleman, A., 1983. Material rate dependence and localized deformation in crystalline solids. Acta Metall. 31, 1951–1976.

Peirce, D., Shih, C.F., Needleman, A., 1984. A tangent modulus method for rate dependent solids. Comput. Struct. 18, 875–887.

Petch, N.J., 1953. The cleavage strength of polycrystals. J. Iron Steel Inst. London 174, 25–28.

Rashid, S., Nemat-Nasser, S., 1992. A constitutive algorithm for rate-dependent crystal plasticity. Comp. Meths Appl. Mech. Engng. 94, 201–228.

Shu, J.Y., Fleck, N.A., 1998. The prediction of a size effect in micro indentation. Int. J. Solids and Structures 35, 1363–1383.

Shu, J.Y., King, W.E., Fleck, N.A., 1998. Finite elements for materials with strain gradient effects. Int. J. Num. Meth. Engng, in press.

Smyshlyev, V.P., Fleck, N.A., 1996. The role of strain gradients in the grain size effect for polycrystals. J. Mech. Phys. Solids 44, 465–495.

Specht, B., 1988. Modified shape functions for the three node plate bending element passing the patch test. Int. J. Num. Meth. Engng. 26, 705–715.

van der Giessen, E., Needleman, A., 1995. Discrete dislocation plasticity: a simple planar model. Modelling Simul. Mater. Sci. Eng. 3, 689–735.

Wei, Y., Hutchinson, J.W., 1997. Steady state crack growth and work of fracture for solids characterised by strain gradient plasticity. J. Mech. Phys. Solids 45, 1253–1273.

William, K., Dietsche, A., Iordache, M.-M., Steinmann, P., 1995. Localisation in micropolar continua. In: Muhlhaus (Ed.), Continuum Models for Materials with Microstructure. John Wiley and Sons, Chichester, U.K.

Xia, Z.C., Hutchinson, J.W., 1996. Crack tip fields in strain gradient plasticity. J. Mech. Phys. Solids 44, 1621–1648.

Zienkiewicz, Z.C., Taylor, R.L., 1994. The Finite Element, vol. 2, 4th ed. McGraw-Hill.